Holocene volcanic activity in Anjouan Island (Comoros archipelago) revealed by new Cassignol-Gillot groundmass K–Ar and ^{14}C ages

Xavier Quidelleur [a,*], Laurent Michon [b,c], Vincent Famin [b,c], Marie-Charlotte Geffray [a], Martin Danišík [d], Nicholas Gardiner [e], Anaïs Rusquet [b,c], Mohamed Gou Zakaria [f]

[a] Université Paris-Saclay, CNRS, GEOPS, Orsay, 91405, France
[b] Université de Paris, Institut de Physique Du Globe de Paris, CNRS, UMR 7154, Paris, 75005, France
[c] Université de La Réunion, Laboratoire GéoSciences Réunion, Saint Denis, 97744, France
[d] John de Laeter Centre, Curtin University, Perth, WA, 6845, Australia
[e] School of Earth and Environmental Sciences, University of St. Andrews, St. Andrews KT16 9AL, UK
[f] Département Sciences de La Terre DST, Laboratoire D'hydrogéologie. Université D'Antananarivo, BP 906, Madagascar

ABSTRACT

The Comoros archipelago has attracted renewed attention since 2018 due to the submarine volcano growing east of the island of Mayotte and the associated ongoing seismic crisis. However, the origin of Comorian magmatism remains controversial, as it is either interpreted as related to a hotspot trail, to a fracture zone, or to a plate boundary. Lying in the central part of the archipelago, Anjouan is a key island to better understand the rela-tionship between volcanism and geodynamics. Together with a careful selection of published whole-rock K–Ar ages, our new set of 13 groundmass K–Ar ages on lava flows and one radiocarbon age on a charcoal from a strombolian deposit, allow us to reassess the volcano-tectonic evolution of Anjouan Island. New groundmass K–Ar ages lie within the last 1 Ma, i.e. from 899 ± 14 to 11 ± 1 ka. They suggest that most of the subaerial volcanism in Anjouan is much younger than previously inferred, and occurred as pulses at 900–750 ka, perhaps 530 ka, 230–290 ka, and since 60 ka, with erosional periods in between. Among our new data, one ^{14}C age of 7513–7089 yrs calBCE (9.3 ± 0.2 ka) and five K–Ar ages younger than 60 ka show that recent volcanism occurred in Anjouan. Moreover, the concentration of eruptive vents along a N150° alignment, parallel to the maximum horizontal stress, suggests a strong link between regional tectonics and volcanism. Considering the presence of active volcanoes on both the western and eastern extremities of the Comoros archipelago, our discovery of Holocene activity on Anjouan provides strong arguments against a chronological progression of volcanism along the archipelago, and therefore contradicts the hotspot hypothesis for the origin of volcanism.

Finally, this study provides a robust geochronological timeframe of the different volcanic stages of Anjouan. It demonstrates that Anjouan is an active island and suggests that volcanism and tectonics can both resume at any time.

1. Introduction

The Comoros archipelago (from west to east: Grande Comore, Mohéli, Anjouan, and Mayotte; Fig. 1a) has gained recent interest from the volcanological community due to the birth of a fast-building submarine volcano east of Mayotte (Cesca et al., 2020; Lemoine et al., 2020; Feuillet et al., 2021). Despite a century of study (e.g., Lacroix, 1922), the origin of Comorian volcanism still remains controversial, with several hypotheses put forward. An east-to-west propagating hotspot track, related to mantle plume magmatism over a moving lithosphere, has frequently been invoked (Hajash and Armstrong, 1972; Emerick and Duncan, 1982; Class et al., 2005). This hypothesis is mainly supported by the apparent westward younging of volcanism from Mayotte (eroded and fringed by a coral reef) to Grande Comore (hosting an active volcano), and by the isotopic signature of Grande Comore magmas. Alternatively, the magmatism of the Comoros archipelago has been interpreted as due to an intraplate fracture zone involving reactivation of lithospheric structures (Nougier et al., 1986). More recently, the magmatism has been proposed to result from lithospheric deformation at the northern boundary of the Lwandle plate (Famin et al., 2020),

* Corresponding author.
E-mail address: xavier.quidelleur@universite-paris-saclay.fr (X. Quidelleur).

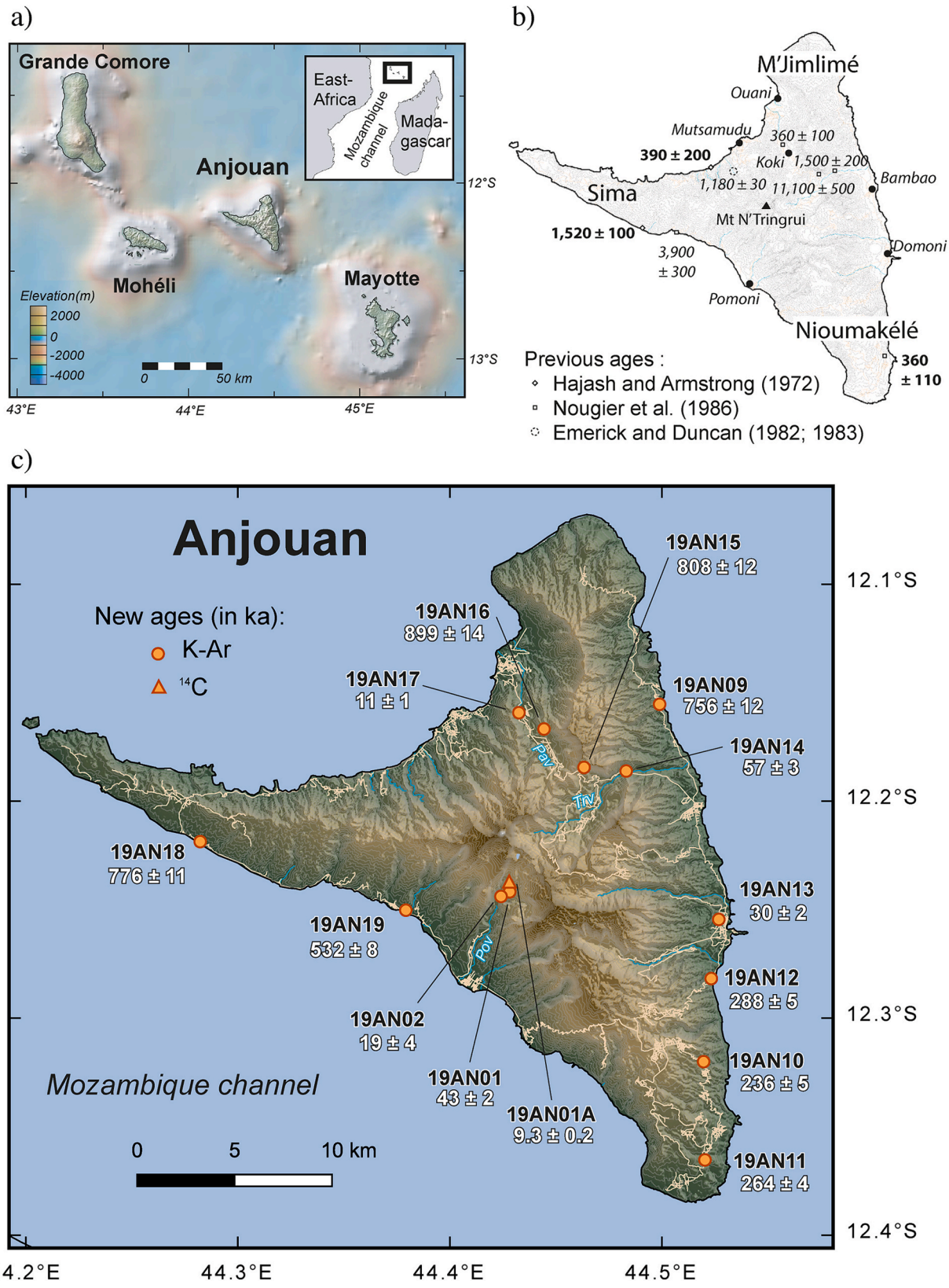

Fig. 1. a) Top-left: Map of the Comoros archipelago with its location relative to Africa and Madagascar shown in insert. Image was made using GeoMapApp. b) Top-right: Map of Anjouan Island showing geographic names and literature K–Ar ages (in Ma). Ages in italic are considered as unreliable (see section 5.1). Note that the sample dated by Emerick and Duncan (1982; 1983) is a poorly located isolated boulder. c) Bottom: Location map of dated samples (orange symbols) from this study. Age and uncertainty are given in ka. The shaded digital elevation model of Anjouan was drawn using QGIS software and topographic data from the Japan Aerospace Exploration Agency. Data for rivers (in blue) and roads (in beige) locations are from OpenStreet (Pav: Patsy river; Trv: Tratinga river; Pov: Pomoni river).

which might be located in the prolongation of the East African Rift System (Michon, 2016).

Before these models can be further investigated, an accurate geochronological framework is mandatory. The radiometric ages published on the Comoros archipelago (reviewed in Michon, 2016) are unevenly distributed, most of them coming from Mayotte (33 K–Ar whole rock ages by Hajash and Armstrong, 1972, Emerick and Duncan, 1982, and Nougier et al., 1986, and 25 $^{40}Ar/^{39}Ar$ ages by Debeuf, 2004 and Pelleter et al., 2014). Only a couple of ages are available on Grande Comore, ten are on Mohéli, and only eight ages have been published on Anjouan (Hajash and Armstrong, 1972; Emerick and Duncan, 1982, 1983; Nougier et al., 1986). Moreover, the latter ages have all been obtained using whole-rock K–Ar dating, which has been shown to be sometime inaccurate due to the incorporation of extraneous ^{40}Ar present in inclusions of mafic minerals, or to the analysis of undetected weathered phases (e.g., Quidelleur et al., 1999).

As ongoing volcanic activity is present at both the western and eastern ends of the Comoros, in Grande Comore at Karthala volcano and offshore east of Mayotte, respectively, it is strategic to focus on Anjouan, the central island of the archipelago. Moreover, morphological evidence such as uneroded eruptive vents suggests the occurrence of a very recent, but yet undated volcanism on this island (de Saint-Ours, 1960), which could have strong implications for regional geodynamics and hazard assessment.

The objective of this study is to develop a more robust geochronological framework of the different volcanic stages of Anjouan by providing radiometric ages of the youngest episodes identified on this island. For this purpose, we have used the Cassignol-Gillot K–Ar dating technique applied to groundmass, and radiocarbon dating applied to charcoal found in volcanic deposits.

2. Geological setting

The nature of the basement beneath the Comoros archipelago has been debated due to the presence of abundant xenoliths of sedimentary rocks of continental origin in volcanic products from all the islands of the archipelago (Lacroix, 1922). Xenoliths of metamorphic and plutonic rocks (Lacroix, 1922) in Anjouan and the occurrence of a large massif of quartzite found in the island central part (Esson et al., 1970; Flower and Strong, 1969; Montaggioni and Nougier, 1981) are additional evidences of continental flavors. Continental fragments under the Comoros archipelago may be remnants of the Gondwana crust, before the breakup of Madagascar and India from Africa in the Early Jurassic (e.g., Courtillot et al., 1999). However, the identification of sea-floor spreading magnetic anomalies in the underlying Comoros crust suggests that the archipelago developed in the vicinity of an oceanic basement (Rabinowitz et al., 1983). Therefore, it has been proposed that these continental rocks may come from the Davie ridge where sediments from the African continent accumulated, and were later displaced towards the Comoros archipelago (Montaggioni and Nougier, 1981). Yet, the origin of these xenoliths of continental sedimentary rocks remains presently unestablished.

The geochemistry of Comorian subaerial lavas shows that magmas are generated with different degrees of partial melting, resulting from plume-lithosphere interaction (Deniel, 1998; Claude-Ivanaj et al., 1998; Class et al., 1998). Sr–Nd–Pb isotopic variations of Grande Comore lavas reflect interaction between a deep mantle plume and the shallow lithospheric mantle (Class and Goldstein, 1997). Helium isotopic analyses also point to the existence of a Comoros plume, suggesting recent mixing between mantle and lithospheric melts (Class et al., 2005). The comparison of magmas isotopic signatures from Karthala and La Grille, the two volcanoes of Grande Comore, suggests that both components might be variable and that the lithospheric component may include a HIMU contribution from delamination or thermal erosion of a continental lithosphere during Gondwana breakup (Pelleter et al., 2014; Bachèlery and Hémond, 2016\).

The morphology of Anjouan is characterized by an overall triangular shape and the presence of the Sima, Jimlimé and Nioumakélé peninsulas, to the west, north and south, respectively (Fig. 1b). The center of the island is made of high reliefs, including Mt N'Tringui the highest summit (1595 m asl), with highly incised and amphitheater-headed valleys. Lava flows are filling some of these valleys, and numerous well-preserved cinder cones and maars are observed throughout the island. Both morphologies support the existence of a relatively recent, post-erosional volcanism in Anjouan (de Saint-Ours, 1960). Three volcanic stages have been proposed for the construction of Anjouan (Flower, 1972). Volcanism started with a shield-building stage outcropping in the central part, with mainly basaltic lavas, including ankaramites, rare hawaiites, and more differentiated lavas. This was followed by an along-rift eruptive stage, which formed the three peninsulas, with basaltic lavas and occasional intercalated pyroclastics. Finally, following an erosional interval, a rejuvenescent stage occurred, with lava flows invading the deeply-incised valleys and flooding the coastal areas. The magma compositions of this last stage belong to the alkaline undersaturated series, with basanites and more differentiated lavas such as phonolites. Previous whole-rock K–Ar ages obtained for Anjouan's lavas range from 3900 ± 300 to 360 ± 100 ka (Hajash and Armstrong, 1972; Emerick and Duncan, 1982, 1983; Nougier et al., 1986). These data, however, are insufficient to place quantitative age limits on these volcanic stages.

A recent detailed morpho-bathymetric study has revealed the submarine volcanic structures within the whole archipelago (Tzevahirtzian et al., 2021). Volcanic ridges are observed between the Comoros Islands and are interpreted as lithospheric fractures controlling the volcanism along a right-lateral transform boundary between the Somalia and Lwandle plates (Famin et al., 2020). This morpho-bathymetric study has also highlighted the existence of hummocky surfaces, intersected by large channels on the submarine flanks of Grande Comore, Mohéli and Anjouan islands. These surfaces have been interpreted as debris avalanche deposits, resulting from large flank collapses, producing scars that can be tentatively identified on-land. Anjouan was probably affected by at least two of these events; a SW directed collapse producing debris avalanche deposits that extend over more than 40 km off-shore, and a NNW collapse with a poorer bathymetric resolution but with an associated on-land concave-shaped morphology (Tzevahirtzian et al., 2021).

3. Sampling

Lava flows from the three volcanic stages previously reported for Anjouan Island have been sampled in spring 2019. Four samples correspond to lava flows that built the largest massifs attributed to the shield building stage (19AN19, 19AN16, 19AN15 and 19AN09). Four samples are located along the western and southern peninsulas: one along the western Sima (19AN18) rift zone and three along the southern Nioumakélé (19AN10, 19AN11 and 19AN12) rift zone. Five samples belong to the recent stage (19AN01, 19AN02, 19AN13, 19AN14 and 19AN17; Fig. 1c). Samples 19AN01 and 19AN02 are from lava flows filling the upper part of the Pomoni valley west of the island central part. Sample 19AN13 is from a lava flow extended in the eastern coastal area around Domoni. This lava flow, which likely originates from well visible craters on the right bank of the valley, unconformably covers the largest maar structure observed in Anjouan. Sample 19AN14 is from a lava flow sequence filling the Tratringa valley. It was sampled just above the Tratringa fall, on the left bank of the river. Sample 19AN17 comes from the massive lava flow filling the Patsy paleo-valley toward the north. All the samples have a porphyric texture with a variable amount of olivine, pyroxene, plagioclase and amphibole phenocrysts (Fig. Sup. Mat. 1). Ultra-mafic and continental xenoliths are found in some of them, notably in 19AN02 and 19AN14 samples.

In addition, one charcoal (labelled 19AN01A) was sampled for radiocarbon dating. The outcrop where the charcoal was extracted

displays a succession of tephra deposits that can be subdivided in three units (Fig. 2). The basal reddish unit (U1), located above lava flow 19AN01, is made of lateritized strombolian deposits, cut and offset by normal faults. U1 is overlain by a dark strombolian unit (U2) at the base of which was found the dated charcoal. U2 has a fan shape filling the trough made by faults in U1. Moreover, this unit is at the same time cut by normal faults but also covers some of them. All these features indicate that the deposition of U2 was coeval with normal faulting. The uppermost unit (U3) is a grayish strombolian layer deposited in unconformity over U2, in which unfortunately no charcoal could be found. U3 is unaltered and barely covered by a few centimeters of soil. U3 also caps the major normal fault cutting U1 and U2.

4. Methods

4.1. K–Ar and ^{14}C dating

Samples for K–Ar dating were selected on the basis of a careful thin section examination. Due to the rock texture (Fig. Sup. Mat. 1), we selected the 125–250 μm size-fraction in order to obtain a homogeneous groundmass preparation without phenocrysts. Heavy liquids were used to isolate a narrow density range of the groundmass and to eliminate possible undetected traces of weathering.

Duplicate potassium (K) and argon (Ar) measurements were performed in the GEOPS laboratory (Université Paris-Saclay, France) using the unspiked Cassignol-Gillot technique (e.g., Gillot et al., 2006). A detailed description of the procedure followed here and uncertainties calculation can be found in Germa et al. (2011). Potassium content was determined by flame spectroscopy using an Agilent AA240 spectrometer operating in absorption mode. Measurements were calibrated using K solutions with concentration ranging from 1 to 2 mg/l and compared to reference standards MDO-G (K 3.510%; Gillot et al., 1992) and BCR-2 (K 1.481%; Raczek et al., 2001). Argon was measured using a multi-collector 180° sector mass spectrometer similar to the one described in Gillot and Cornette (1986). The unspiked Cassignol-Gillot technique is based on comparison of argon isotopes 36 and 40 from atmospheric and sample aliquots. The air pipette was calibrated by routine measurements of HD-B1 standard (Fuhrmann et al., 1987) using the age of 24.18 Ma (Schwarz and Trieloff, 2007). K isotopic ratios and ^{4}K decay constants of Steiger and Jager (1977) have been used. All uncertainties reported in this study are quoted at the 1σ level (Table 1).

Radiocarbon dating was performed on a charcoal sample prepared in the Center de Datation par le Radiocarbone at Lyon (France), and measured using a MICADAS accelerator mass spectrometer at University of Groningen (Netherlands).

4.2. Major and trace elements

Following powder grinding, major and trace element whole-rock contents of all samples were measured in the Laboratoire Géosciences Océan (Université de Bretagne Occidentale, France) by ICP-AES (Inductively Coupled Plasma - Atomic Emission Spectrometry), following the analytical procedure detailed in Cotten et al. (1995). Relative uncertainties are lower than 2% for major elements and lower than 5% for trace elements. Data are provided in Table 2.

5. Results

5.1. K–Ar and ^{14}C ages

We have obtained thirteen new K–Ar ages ranging from 899 ± 14 to 11 ± 1 ka (Table 1 and Fig. 1c). Potassium content of the groundmass ranges between 1.138% and 2.925% and radiogenic ^{40}Ar content between 0.5% and 27.8%. Five ages are younger than 100 ka (19AN01, 19AN02, 19AN13, 19AN14 and 19AN17). They all correspond to lava flows that partially filled the deep valleys incised in the old massif. Three ages, obtained along the southern Nioumakélé peninsula, cluster ca. 250 ka (19AN10, 19AN11, 19AN12). Four ages fall within the 750–900 ka range (19AN09, 19AN15, 19AN16 and 19AN18). Their spatial distribution reveals a period of construction that contributed to the building of the Sima ridge and the inner massifs that have been subsequently dissected by erosion. One age seems isolated at 532 ± 8 ka (19AN19), in between the latter two groups. Whether this age represents a distinct period of construction or witnesses a single eruption cannot be determined with our data.

The charcoal sampled above lava flow 19AN01 yielded a ^{14}C age of 8335 ± 50 yrs BP, which, once calibrated (Hogg et al., 2020), falls within a 2σ age range of 7513–7089 yrs calBCE (ca. 9.3 ± 0.2 ka).

5.2. Major and trace elements

Major and trace elements analyses have been performed for all dated rocks from this study (Table 2). For the sake of comparison, we have completed our dataset using the Georoc database with major elements analyses obtained from whole-rock volcanic rocks from Anjouan (Flower, 1971; 1973; Thompson and Flower, 1971; Nougier et al., 1986), Grande Comore (Class and Goldstein, 1997; Class et al., 1998, 2005; Claude-Ivanaj et al., 1998; Deniel, 1998; Flower, 1971; Spath

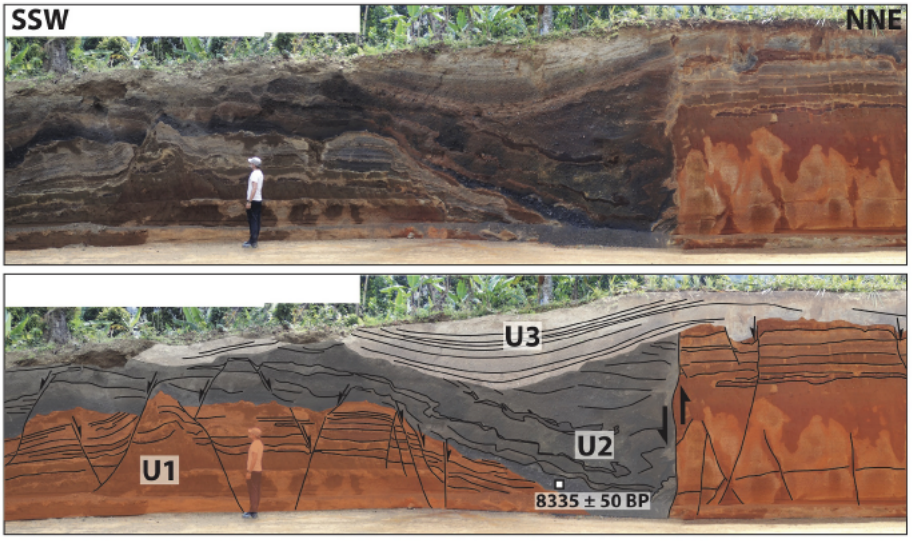

Fig. 2. Outcrop on a road cut where the charcoal 19AN01A was collected (lat. 12.2416691; lon. 44.428049), about ~10 m above the lava flow 19AN01. The outcrop can be subdivided into three units. U1 is a lateritized strombolian deposit cut by normal faults. U2, also a strombolian deposit to which belongs the charcoal, is barely altered and deposited in unconformity over U1. U2 is at the same time cut by some normal faults and covers others. U3 is an unaltered strombolian deposit in unconformity over U2, masking normal faults.

Table 1
New K–Ar ages performed on groundmass separates. Column headings indicate sample names; latitude (in degrees); longitude (degrees); potassium (K) concentration in percent; concentration of radiogenic ^{40}Ar ($^{40}Ar^*$) in percent; concentration of radiogenic ^{40}Ar ($^{40}Ar^*$) $\times 10^{11}$ in number of atoms per gram; age (in ka); 1-sigma uncertainty (Un., in ka); weighted mean age (in ka); 1-sigma weighted uncertainty (in ka).

Sample	Lat. (°)	Long. (°)	K (%)	$^{40}Ar^*$ (%)	$^{40}Ar^*$ (10^{11} at/g)	Age (ka)	Un. (ka)	Mean Age (ka)	±1 σ (ka)
19AN01	−12.24167	44.42805	1.537	1.9	0.68602	43	2		
				1.7	0.70457	44	3	**43**	**2**
19AN02	−12.24384	44.42442	1.673	0.5	0.33721	19	4		
				0.5	0.31693	18	4	**19**	**4**
19AN09	−12.15533	44.49889	1.172	17.6	9.2540	756	12		
				17.5	9.2667	757	12	**756**	**12**
19AN10	−12.32003	44.51970	1.275	7.3	3.1743	238	5		
				7.3	3.1248	235	5	**236**	**5**
19AN11	−12.36509	44.51483	2.036	14.2	5.6123	264	4		
				13.5	5.6072	264	4	**264**	**4**
19AN12	−12.28174	44.52328	1.539	10.6	4.5770	285	5		
				11.1	4.6873	292	5	**288**	**5**
19AN13	−12.25464	44.52706	1.786	1.3	0.57298	31	2		
				1.4	0.53286	29	2	**30**	**2**
19AN14	−12.18610	44.48324	1.582	2.1	0.92654	56	3		
				2.0	0.96222	58	3	**57**	**3**
19AN15	−12.18454	44.46301	1.282	25.5	10.917	815	12		
				25.4	10.732	801	12	**808**	**12**
19AN16	−12.16665	44.44430	1.138	15.3	10.725	902	14		
				14.5	10.665	897	14	**899**	**14**
19AN17	−12.15918	44.43271	2.925	1.3	0.36091	12	1		
				1.4	0.31962	10	1	**11**	**1**
19AN18	−12.21951	44.28131	1.381	27.5	11.230	779	11		
				27.8	11.164	774	11	**776**	**11**
19AN19	−12.25041	44.37912	2.201	20.8	12.241	533	8		
				21.2	12.1982	531	8	**532**	**8**

Table 2
Major (in %) and trace elements (in ppm) composition of whole-rock samples dated here. L.O.I: loss on ignition.

	19AN01	19AN02	19AN09	19AN10	19AN11	19AN12	19AN13	19AN14	19AN15	19AN16	19AN17	19AN18	19AN19
Wt.%													
SiO_2	44.12	43.80	43.79	43.17	45.34	45.76	45.68	44.90	47.05	45.13	53.39	45.88	49.66
TiO_2	2.68	2.73	2.67	2.75	2.83	2.15	2.63	2.66	2.97	2.47	0.77	2.87	1.53
Al_2O_3	15.22	14.62	12.14	12.83	15.51	14.29	16.46	15.74	14.76	11.66	19.00	14.43	17.63
Fe_2O_3	14.14	14.44	14.30	13.89	13.74	12.63	14.06	14.06	13.87	14.06	9.85	13.76	11.66
MnO	0.22	0.22	0.18	0.19	0.22	0.19	0.24	0.22	0.19	0.18	0.25	0.19	0.23
MgO	6.93	7.80	10.72	10.14	5.15	7.93	4.09	5.97	5.92	11.72	1.05	6.57	2.29
CaO	9.66	9.90	10.74	10.81	7.02	9.58	8.32	9.20	9.62	10.24	4.16	9.07	5.98
Na_2O	4.71	4.50	2.43	3.30	6.34	4.84	5.08	5.06	3.75	2.55	8.46	4.05	6.73
K_2O	1.75	1.59	1.14	1.20	2.49	1.79	2.02	1.93	1.39	1.04	3.34	1.61	2.59
P_2O_5	0.88	0.85	0.49	0.66	0.84	0.53	1.09	0.85	0.57	0.44	0.45	0.74	0.99
L.O.I.	−0.81	−0.74	1.73	1.13	0.25	0.23	0.08	−0.69	0.06	0.33	−0.08	0.12	1.05
Total	99.50	99.69	100.33	100.06	99.73	99.92	99.75	99.90	100.14	99.82	100.63	99.30	100.34
Ppm													
Ba	573	536	346	488	937	572	693	557	378	275	961	450	915
Ce	100	94	63	86	147	78	112	96	78	57	131	92	195
Dy	6.17	5.97	4.79	5.41	6.76	4.72	6.93	5.74	5.73	4.81	5.30	5.67	7.34
Er	2.75	2.69	1.99	2.24	3.11	2.14	3.07	2.62	2.49	2.05	2.76	2.38	3.39
Eu	3.0	3.0	2.3	2.9	3.6	2.4	3.5	2.8	2.7	2.2	2.8	3.0	4.1
Gd	8.9	8.4	6.7	8.1	10.2	6.7	10.1	8.0	7.9	6.5	7.5	8.5	11.8
Hf	4.49	4.29	4.12	4.42	5.54	4.47	4.72	4.59	5.61	4.36	6.46	6.10	9.02
Ho	1.13	1.09	0.84	0.95	1.24	0.87	1.26	1.06	1.03	0.86	1.03	1.00	1.35
La	52	49	32	44	83	42	57	50	39	28	77	47	110
Lu	0.34	0.33	0.23	0.25	0.41	0.27	0.37	0.32	0.29	0.24	0.42	0.28	0.45
Nb	96	88	58	78	144	85	103	94	80	57	132	90	177
Nd	47	45	32	43	60	35	55	44	39	30	47	45	77
Pb	3.78	3.42	3.14	3.78	10.00	4.68	3.97	4.38	3.12	2.29	11.86	3.93	9.62
Rb	31	31	24	26	57	40	36	21	24	23	79	36	76
Sm	8.9	8.8	6.8	8.5	10.6	6.8	10.5	8.4	7.9	6.5	7.7	9.0	12.5
Sr	718	688	510	694	1053	664	890	640	504	412	846	657	1190
Ta	10.7	9.9	7.0	9.0	15.7	9.8	11.0	10.7	9.9	7.0	15.7	10.9	21.3
Tb	1.25	1.20	0.97	1.12	1.39	0.95	1.42	1.15	1.15	0.96	1.05	1.18	1.55
Th	5.20	4.79	3.30	4.80	12.16	4.99	4.54	4.64	4.29	2.98	11.46	4.97	13.78
Tm	0.38	0.37	0.27	0.30	0.44	0.30	0.42	0.37	0.34	0.28	0.42	0.33	0.49
U	1.27	1.14	0.83	1.09	2.67	1.28	0.96	1.41	1.13	0.78	2.03	1.30	4.15
Y	28.93	27.61	20.73	24.19	32.99	21.90	32.02	26.46	26.29	21.44	27.46	25.51	35.59
Yb	2.41	2.33	1.65	1.83	2.85	1.89	2.64	2.28	2.12	1.74	2.86	2.02	3.21
Zr	231	217	202	225	320	243	236	248	284	210	392	322	549

et al., 1996; Strong, 1972), Mohéli (Nougier et al., 1986; Spath et al., 1996; Strong, 1972), and Mayotte (Nougier et al., 1986; Pelleter et al., 2014; Spath et al., 1996).

The total alkali versus silica (TAS) diagram (Fig. 3) shows that most of our 13 samples are relatively basic with SiO_2 contents lower than 48% for 9 tephrites-basanites, one basalt (19AN16) and one trachy-basalt (19AN15). Only samples 19AN19 and 19AN17 display a higher degree of differentiation and plot in the phono-tephrite and tephri-phonolite fields, respectively. Overall, they fall within the range of the Comoros lavas, mostly belonging to the basalt and trachy-basalt fields, and to the silica undersaturated series.

Spider diagrams of trace elements analyses normalized to primitive mantle and Rare Earth elements (REE) normalized to chondrite (Sun and McDonough, 1989) are shown in Fig. 4a and b. Overall, they present patterns and values typical of those observed for Comorian lavas (e.g., Deniel, 1998; Pelleter et al., 2014; Spath et al., 1996), with minor depletions in Pb and Hf, and small enrichments in Nb and Ta. Three subsets can be distinguished within our dataset. Samples 19AN09 and 19AN16 are slightly depleted in most trace elements, while samples 19AN11, 19AN17 and 19AN19 are slightly enriched. The crystal contents are relatively high for the former subset, while only rare phenocrysts (e.g. amphiboles in 19AN17) present in a fine-grained matrix are observed in the latter (Fig. Sup. Mat. 1). A clear enrichment in light-REE compared to heavy-REE is observed in Fig. 4b, suggesting a moderate to low degree of mantle partial melting (Rollinson, 1993). As above, samples 19AN09 and 19AN16, display lower values, while samples 19AN11, 19AN17 and 19AN19 have slightly higher REE contents than others.

6. Discussion

6.1. Comparison with earlier studies

Hajash and Armstrong (1972) reported 2 whole-rock K–Ar ages from Anjouan (Fig. 1b), as well as 29 paleomagnetic directions from distinct lava flows. An age of 390 ± 200 ka was obtained along the northwestern coast, in a location that we did not investigate, and the second age of 1520 ± 100 ka comes from the southwest part of the Sima peninsula. This latter age agrees with its reverse paleomagnetic polarity, but this does not prevent any age overestimation, as often observed with whole-rock K–Ar (e.g., Samper et al., 2007). Note that we have obtained

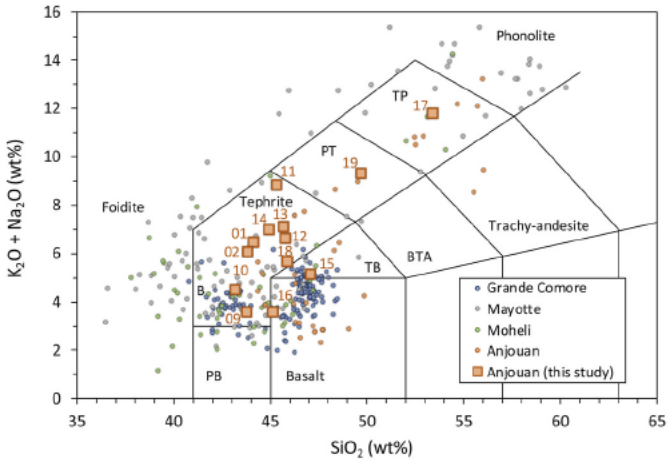

Fig. 3. The total alkali versus silica (TAS) diagram for rocks from the Comoros Islands. Data have been extracted from the Georoc database (see text for references). The large orange square symbols are for samples from this study, with the number above each corresponding to sample name. Samples from previous studies are shown with small circles with a given color for each island. Rock fields are from Le Bas et al. (1986). PB: Picro-basalt; B: Basanite; TB: Trachy-basalt; BTA: Basaltic trachy-andesite; PT: Phono-tephrite; TP: Tephri-phonolite.

a significantly younger age of 776 ± 11 ka for 19AN18, located only 4 km away from Hajash and Armstrong's sample (Fig. 1b). Within uncertainty, our age is also compatible with a reverse polarity from the end of the Matuyama chron (e.g., Quidelleur et al., 2003). Hajash and Armstrong's sample and ours are located on similar geomorphological features of the southern Sima peninsula slope and should be of similar ages instead of the factor of two discrepancy obtained here. Although we cannot completely exclude it, such a comparison strongly casts suspicion on the validity of Hajash and Armstrong's whole-rock age.

A single K–Ar whole-rock age of 1180 ± 30 ka is reported for the northwestern part of Anjouan (Fig. 1b) by Emerick and Duncan (1982; 1983). However, its description as a stream cobble makes its stratigraphic position unknown and implies to consider this age only as possibly recording a volcanic period.

Five whole-rock K–Ar ages were obtained in Anjouan by Nougier et al. (1986), with two of them allowing a direct comparison with our new ages (Fig. 1b). Their sample AN02 (K% 1.53) is from the Tratringa valley flow, as is our sample 19AN14 (K% 1.58), both taken at the Tratringa fall. However the two ages strongly differ (1500 ± 200 ka for AN02 and 57 ± 3 ka for 19AN14). The presence of numerous mantle xenoliths found in this lava, which carry a lot of ^{40}Ar in excess, probably led to the over-estimated whole-rock K–Ar age of 1500 ± 200 ka in Nougier et al. (1986). Note that sample 2 of Hajash and Armstrong (1972), also from the same locality, which is the only flow along the road in this area, carries a normal polarity. This is in full disagreement with such an age of 1500 ± 200 ka, which should be associated with a reverse polarity from the Matuyama chron. Conversely, carefully selected groundmass from our sample 19AN14 (Fig. 1c) allowed us to obtain a much younger age of 57 ± 3 ka, which is in agreement with the normal polarity as obtained by Hajash and Armstrong (1972). Hence, our age most probably corresponds to this valley flow, which is weakly eroded and forms a knickpoint on the river profile. Another direct comparison can be made with the massive Patsy paleo-valley flow forming the valley floor, which is currently incised by the river. Nougier et al. (1986) obtained a whole-rock age of 360 ± 100 ka for this tephri-phonolite lava (AN01; K% 2.76), while we obtained our youngest age of 11 ± 1 ka on the groundmass of this lava (19AN17; K% 2.92; Fig. 1). As it is not possible to obtain a too young K–Ar age in the absence of strong re-heating events, the above comparisons further show that too old ages are commonly obtained by whole-rock dating. This is further illustrated by the age of 3900 ± 300 ka (AN08; Nougier et al., 1986), obtained on the southwest coast (Fig. 1b). Although no direct comparison can be proposed here, we note that at the same location, the three flows 25, 26 and 27 of Hajash and Armstrong (1972) carry a normal polarity. Therefore, Nougier's whole-rock age is also in disagreement with the geomagnetic polarity timescale (Cande and Kent, 1995), which shows a Gilbert chron reverse polarity throughout the time interval from 4.2 to 3.6 Ma. Within the southern Nioumakélé peninsula, an age of 360 ± 110 ka has been reported by Nougier et al. (1986). It comes from a lava flow located in between our samples 19AN10 and 19AN11 (Fig. 1c), which have comparable, albeit much more precise ages of 236 ± 5 and 265 ± 4 ka, respectively (Table 1). Finally, Nougier et al. (1986) obtained an age of 11,100 ± 500 ka for a syenite from the Chandra basin (Fig. 1b). However, we think that a whole-rock age for an intrusive rock is meaningless (e.g., McDougall, 1971). Effectively, as intrusive rocks comprise minerals with different closure temperatures, these minerals will have different ages corresponding to the timing of exhumation through the different isotherms. Consequently, this syenite age will not be considered further here.

This direct comparison of whole-rock K–Ar ages with our new groundmass K–Ar ages, as well as, when available, with the polarity of dated lava flows and the geomagnetic polarity time scale, further demonstrates that whole-rock K–Ar ages should be regarded only with great caution. From the above discussion, only four ages from the literature on Anjouan (1520 ± 100, 1180 ± 30, 390 ± 200, and 360 ± 110 ka) are not categorically invalidated, and only one (360 ± 110 ka) is

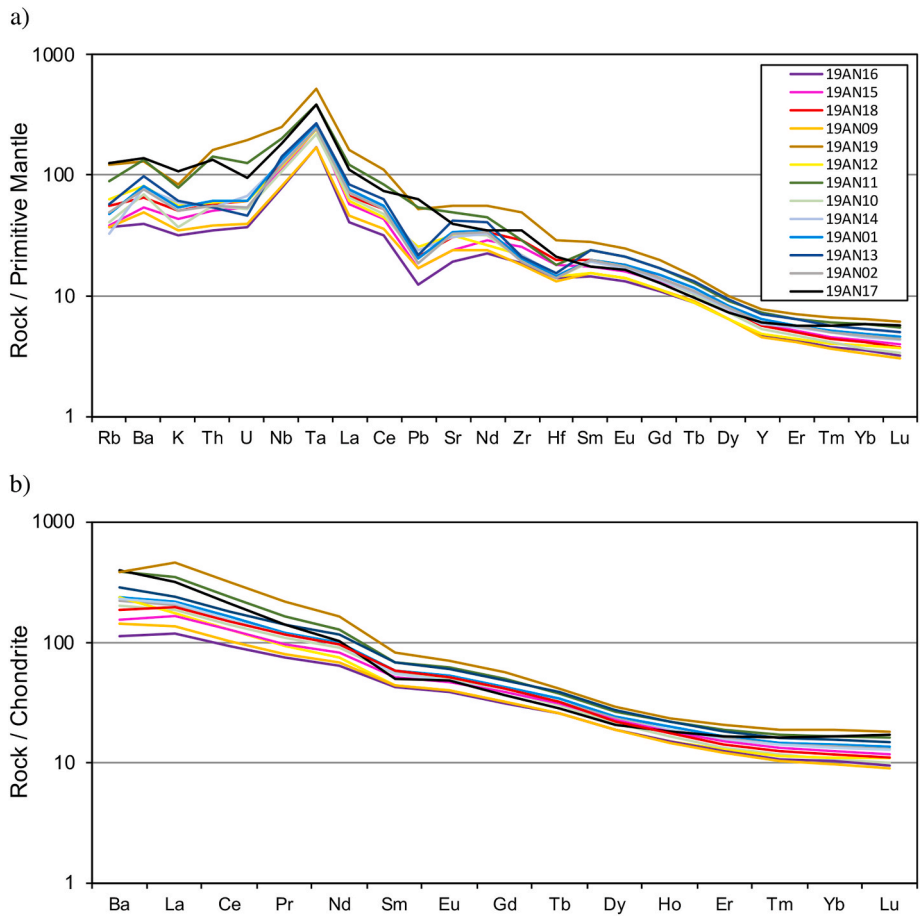

Fig. 4. a) Multi-element patterns normalized to primitive-mantle (after Sun and McDonough, 1989) of the samples used in this study. Note that the legend is sorted from the oldest to the youngest sample. b) Rare Earth Element (REE) patterns normalized to chondrite values (after Sun and McDonough, 1989) for the same samples.

confirmed by our new data.

6.2. *Volcanic evolution of Anjouan*

Using the fourteen new groundmass K–Ar and ^{14}C ages from this study, together with four of the remaining whole-rock K–Ar ages (see above), a total of eighteen radiometric ages is available for Anjouan. In Fig. 5, the age-probability (Deino and Potts, 1992) calculated from this dataset shows that the subaerial history of the Anjouan Island appears

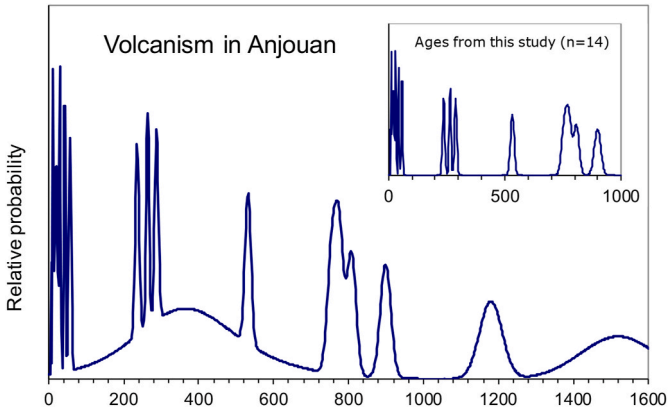

Fig. 5. Age-probability distribution spectra (Deino and Potts, 1992) showing the periods of volcanic activity in Anjouan based on 14 radiometric ages from this study, 2 from Hajash and Armstrong (1972), 1 from Emerick and Duncan (1982) and 1 from Nougier et al. (1986).

younger than previously inferred (e.g., Michon, 2016). Although the sampling might be biased by lacking the oldest units recovered by more recent lavas, this dataset suggests a relatively rapid subaerial construction, especially since 0.9 Ma.

The oldest age we obtained (899 ± 14 ka; 19AN16) comes from a massive fresh angular block, located on top of a remnant plateau dominating the east side of the Patsy valley. This age is puzzling considering the younger age of 808 ± 12 ka of sample 19AN15, located within the wall of a subvertical crest, hence, unambiguously belonging to the old massif. Fig. 6 shows that the small plateau where 19AN16 was sampled seems to belong to the Mt N'Tringrui massif. In such hypothesis, this plateau should be younger than the wall of the old massif dated by sample 19AN15 at 808 ± 12 ka. Consequently, as sample 19AN16 is our only sample not coming from a lava flow in place but was isolated, we suggest that it is actually a block fallen from the old massif.

Based on bathymetry and on-land morphology, Tzevahirtzian et al. (2021) have suggested that Anjouan probably experienced a NW directed flank collapse. The wall of the NNW concave-shaped structure, east of the Patsy valley, might represent the scar of this collapse (Fig. 6). The ages obtained for the old massif that was affected by the collapse range from 899 ± 14 ka (including the presumably fallen block) to 756 ± 12 ka.

More than 200 ka younger, an age of 532 ± 8 ka was obtained for 19AN19 located near the SW coast, within the scar associated with a SW directed flank collapse that could be identified by the bathymetry (Tzevahirtzian et al., 2021). Therefore, it represents an older bound for this second collapse. Moreover, as sample 19AN19 lies on the SW slope of Mt N'Tringrui massif, that seems to be emplaced within the scar of the NW directed flank collapse (Fig. 6), this age might also represent a

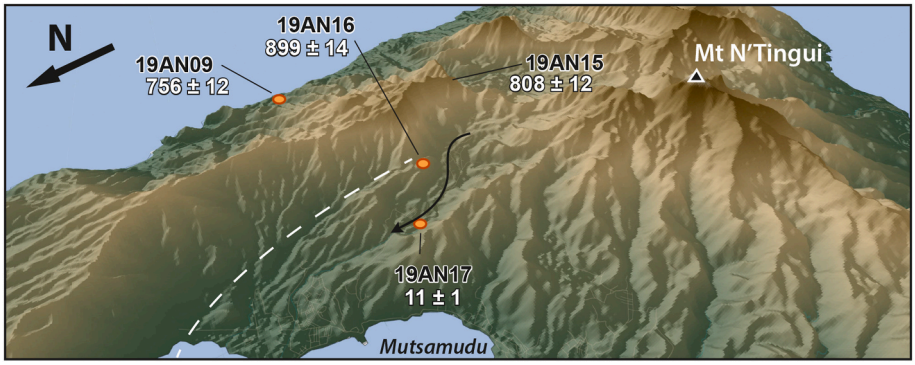

Fig. 6. Perspective view of Anjouan from NW looking SE. The white dashed line indicates the possible location of the scar of the NW directed flank collapse inferred from bathymetry data (Tzevahirtzian et al., 2021).

younger bound for this first collapse.

The three ages obtained for the south appear rather close, between 288 ± 5 and 236 ± 5 ka (Fig. 1). They have been obtained on lava flows emitted from the topographic crest forming the Nioumakélé peninsula. This peninsula also comprises many recent volcanic vents and can be interpreted as a rift zone, where volcanic activity is concentrated along a preferential orientation of N150° (Famin et al., 2020). Note that the whole-rock K–Ar age of 360 ± 110 ka obtained by Nougier et al. (1986) agrees with our new ages given its large uncertainty.

Finally, the youngest ages obtained here (19AN01, 19AN02, 19AN13, 19AN14 and 19AN17), all younger than 57 ± 3 ka, suggest a lull of activity during ~180 ka. They come from lava flows filling erosional valleys and being emitted from vents also lying more or less along the N150° direction (Fig. 7). This suggests a long-lasting influence of the regional tectonics (Famin et al., 2020).

Regarding the chemical evolution of magmatism through time, our data do not display any marked tendency within the last 900 kyr interval (Fig. 8). The SiO_2 content remains in the range of 43–47% for all the samples except 19AN19 and 19AN17, the most evolved rocks, which experienced fractional crystallization to phono-tephrite and tephri-phonolite, respectively (Fig. 8a). The MgO content shows a relatively large dispersion from about 1 to 12%, without a clear temporal evolution, besides the oldest and youngest lavas showing the highest and lowest content, respectively (Fig. 8b). The total alkali contents evolution through time (not shown), which range from 3.57 to 11.8% (Fig. 3), displays the same features, but with the oldest and youngest lavas showing the lowest and highest content, respectively. Similarly, the La/Sm ratio remains within the range of ~3–4 for most basic lavas from this study (Fig. 8c), suggesting a rather constant magmatic source throughout the subaerial activity of Anjouan. This inference requires a more thorough investigation including isotopic analyses, which are beyond the scope of the present study.

Altogether, the ages obtained here and the somewhat homogeneous trace elements patterns observed through time, allow us to propose a rather simple volcanic scheme for Anjouan. The construction of the island started with a main magmatic vent system most probably close to the present center of the island. The associated rift-zones, whose orientations are imposed by the regional tectonics, are observed on-land and offshore (Famin et al., 2020; Tzevahirtzian et al., 2021) and still guide the magmatism towards the surface up to the most recent volcanic activity. The subaerial activity is at least 899 ± 14 ka, or as old as 1520 ± 100 ka if we consider whole-rock K–Ar ages. The activity was characterized by successive periods of volcanic activity that was building the island or filling incised valleys (750–900 ka; perhaps 530 ka; 230–290 ka and since 57 ka), and was separated by periods of erosion that dissected the island reliefs, and by several flank collapses. These events have probably produced the debris avalanche deposits found on the sea floor around the island (Tzevahirtzian et al., 2021).

At a first glance, the shape and volcanic history of Anjouan island appears similar to that of El Hiero in the Canary Islands, with a subaerial volcanic history covering the last ~1 Myr (Guillou et al., 1996), volcanic rift zones converging towards the island center, and large sector collapse scars in-between (Carracedo, 1994; Masson, 1996; Gee et al., 2001).

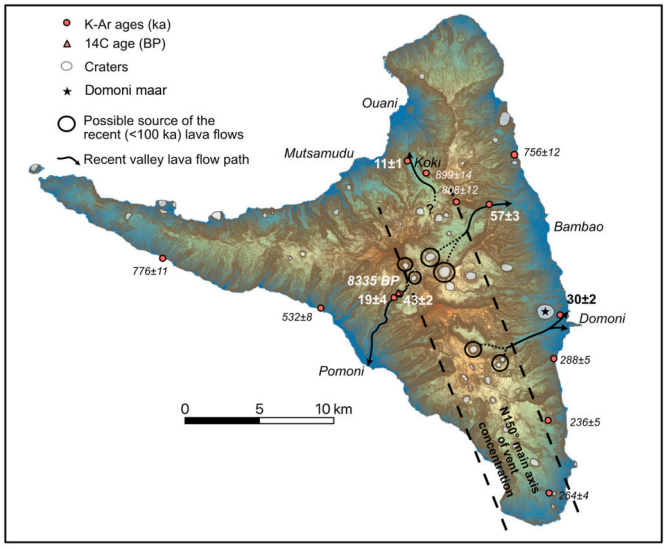

Fig. 7. Topographic map of Anjouan showing new ages from this study as well as recent volcanic features. Craters are shown in grey and Domoni maar is located with a star. Recent valley flow paths are shown with black arrows. The N 150° main axis of vent concentration (Famin et al., 2020) is located within black dashed lines.

6.3. Geodynamic implications

Our discovery of Holocene volcanism in Anjouan, as well as the active volcanism in Grande Comore (Bachèlery et al., 2016), and offshore east of Mayotte (e.g., Bachèlery et al., 2019; Feuillet et al., 2019), either contradicts the age increase that should be observed from Grande Comore to Mayotte in the hot-spot track hypothesis, or suggests that this hotspot leaves an unusual tail of volcanic activity behind the plume head. In addition, recent bathymetry data highlighted morphological features, including the state of erosion of the different islands, and the presence of large insular shelfs in Mohéli and Mayotte, which also disagrees with a continuous eastward aging of these volcanic structures from east to west (Tzevahirtzian et al., 2021). Considering a volume of about 500 km^3 for Anjouan, as modeled by a 2000 m high cone with a basal radius of about 15 km, and a construction of the island during a 1.5 Myr time interval, an output rate of about 3.1×10^{-4} km^3/yr can be calculated. However rough this estimate may be, it is

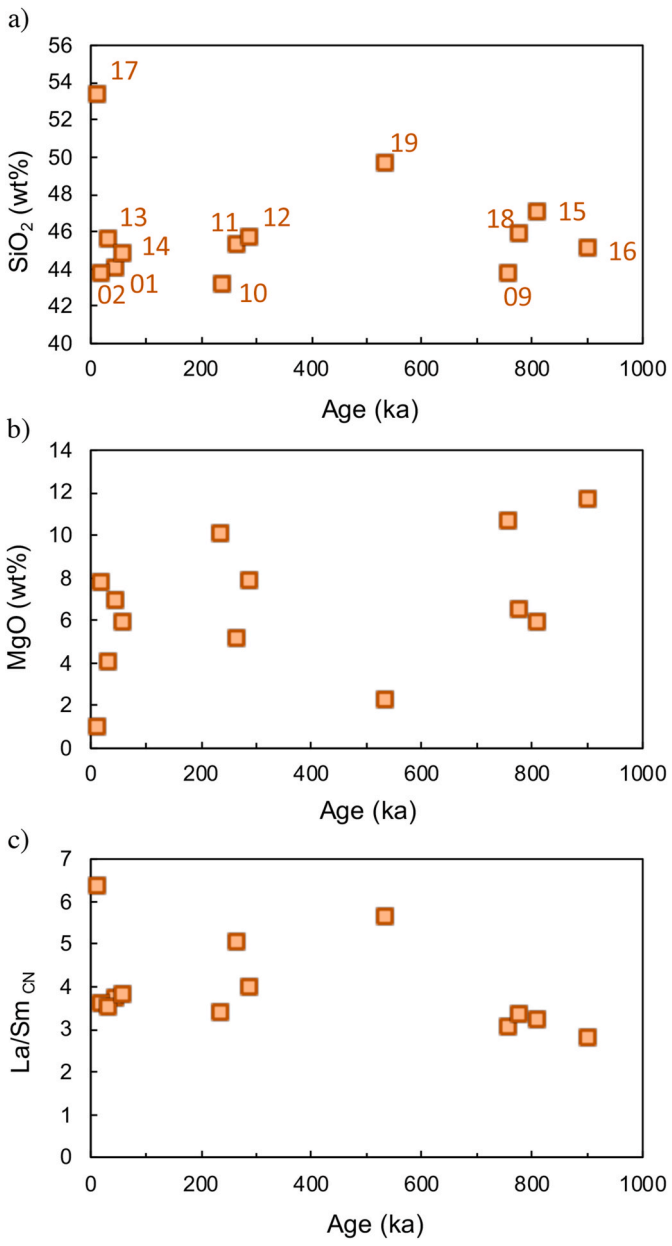

Fig. 8. a) Evolution of SiO_2 content (in weight %), reflecting differentiation, as a function of sample age (in ka). The number above each symbol corresponds to sample name. b) same as a) for MgO. c) Same as a) for the La/Sm ratio, calculated after normalization to chondrite values (after Sun and McDonough, 1989).

much lower than the average value of 10^{-2} km^3/yr observed for oceanic volcanoes, and still an order of magnitude lower than hotspot islands such as La Réunion where output rates of about 2.4×10^{-3} km^3/yr are obtained for a 2 Myr duration (White et al., 2006). However, the output rate that has been calculated for Anjouan is similar to those calculated for continental subduction volcanoes, such as Mojanda volcano in Ecuador (Bablon et al., 2020) or Mt Adams in the Cascades (USA; Hildreth and Lanphere, 1994), for instance. The above considerations suggest that the magmatic production in the Comoros is rather low, which is an additional contradiction to the hotspot hypothesis.

In Anjouan, subaerial volcanic activity for the last 1 Ma, in the time interval where ages are best constrained (Fig. 5), seems to occur as four distinct pulses, separated by ~200 ka-long quiescent intervals. In the absence of reliable radiometric ages for all the Comoros archipelago, it is difficult to interpret such distribution, but its discontinuous nature could reflect faulting activity during deformation phases occurring at the newly forming Somalia-Lwandle plates boundary (Famin et al., 2020). Clearly, new ages of subaerial and submarine volcanics throughout the archipelago are urgently needed.

6.4. *Volcanic and tectonic hazards assessment*

Our new ages also show that volcanism is still ongoing in Anjouan since the Late Pleistocene (<100 ka). Moreover, Holocene volcanism is indicated by two independent radiometric methods on different deposits, the massive Patsy paleo-valley flow dated by K–Ar at 11 ± 1 ka, and the U2 strombolian deposit in the upper Pomoni valley dated by ^{14}C at 9.3 ± 0.2 ka (7513-7089 cal yrs BCE). The U3 unit also implies that even more recent volcanic eruption occurred in the central part of Anjouan during the last thousand years. The second implication revealed by this key outcrop (Fig. 2) is the existence of Holocene faulting and active tectonic activity on Anjouan in the Holocene. Such a short delay since the last eruption and deformation clearly demonstrates that Anjouan is an active island, and that volcanism and tectonics can both resume at any time. Consequently, we propose that Anjouan should now be included in the list of active African volcanoes (e.g. Lenhardt and Oppenheimer, 2014).

Finally, based on the Late Pleistocene - Holocene activity of the island, future eruptions could be characterized as eruption of lava flows emitted from a vent located along the N150° alignment, filling the deeply incised valleys, and eventually flooding coastal plains (Fig. 7). It would therefore represent an important hazard for people and infrastructures, as most inhabitants from this island live in cities located within such valleys or along the coast. Moreover, as several of them, such Domoni, Bambao, Pomoni, Koki and Ouani, for instance, are built onto recent lavas, a future lava flow could eventually follow the same path and be a major threat for the population.

7. Conclusions

Our new groundmass K–Ar and ^{14}C ages lie within the last 1 Ma and suggest that most of the subaerial volcanism in Anjouan is much younger than the 11 to 4 Ma previously inferred. Although the onset of volcanism could not be dated due to the lack of access to basal units, an age of 1520 ± 100 ka (Hajash and Armstrong, 1972) was previously available from K–Ar whole-rock dating. Our new K–Ar groundmass ages show that volcanism occurred as pulses at 900–750 ka, 530 ka (?), 230–290 ka, and since 60 ka. Volcanic episodes were separated by periods of erosion that dissected the island reliefs and by several flank collapses (Tzevahirtzian et al., 2021).

The recent volcanic ages obtained here, together with the present-day active volcanoes on both western and eastern sides of the Comoros archipelago, namely the Karthala volcano on Grande Comore and the submarine volcano off Mayotte's eastern coast, respectively, are strong arguments against the hotspot hypothesis previously proposed. Alternatively, the discontinuity of volcanism throughout the last million years, and the concentration of recent lava flow vents along the N150° alignment, suggest a strong link between regional tectonic activity and volcanism (Famin et al., 2020).

Finally, this study demonstrates that Anjouan is an active island and suggests that volcanism and tectonics can both resume at any time.

Funding

This research was funded by the CNRS/INSU TELLUS "MAYVOLTE" grant.

Declaration of competing interest

The authors declare that they have no known competing financial interests or personal relationships that could have appeared to influence

the work reported in this paper.

Acknowledgements

We thank Nils Lenhardt and Patrick Bachèlery for their detailed review. DEM data have been provided by AW3D of the Japan Aerospace Exploration Agency. OpenStreet Map and MapTiler are also thanked for providing map data used in Figs. 1 and 6. This is LGMT contribution number 167.

Appendix A. Supplementary data

Supplementary data to this article can be found online at https://doi.org/10.1016/j.quageo.2021.101236.

References

Bablon, M., Quidelleur, X., Samaniego, P., Le Pennec, J.L., Santamaría, S., Liorzou, C., Hidalgo, S., Eschbach, B., 2020. Volcanic history reconstruction in northern Ecuador: insights for eruptive and erosion rates on the whole Ecuadorian arc. Bull. Volcanol. 82, 1–23.

Bachèlery, P., Hémond, C., 2016. Geochemical and petrological aspects of Karthala p. 367-384. In: Active Volcanoes of the Southwest Indian Ocean. Springer-Verlag Berlin Heidelberg, p. 428.

Bachèlery, P., Morin, J., Villeneuve, N., Soulé, H., Nassor, H., Ali, A.R., 2016. Structure and eruptive history of Karthala volcano p. 345-366. In: Active Volcanoes of the Southwest Indian Ocean. Springer-Verlag Berlin Heidelberg, p. 428.

Bachèlery, P., Berthod, C., Di Muro, A., Gurioli, L., Besson, P., Caron, B., et al., 2019. Petrological and geochemical characterization of the lava from the 2018-2019 Mayotte eruption: first results. In: AGU Fall Meeting Abstracts, vol. 2019. December vols. 52D-06.

Cande, S.C., Kent, D.V., 1995. Revised calibration of the geomagnetic polarity timescale for the Late Cretaceous and Cenozoic. J. Geophysis. Res.: Solid Earth 100, 6093–6095.

Carracedo, J.C., 1994. The Canary Islands: an example of structural control on the growth of large oceanic-island volcanoes. J. Volcanol. Geoth. Res. 60, 225–241.

Cesca, S., Letort, J., Razafindrakoto, H.N.T., Heimann, S., Rivalta, E., Isken, M.P., Nikkhoo, M., Passarelli, L., Petersen, G.M., Cotton, F., Dahm, T., 2020. Drainage of a deep magma reservoir near Mayotte inferred from seismicity and deformation. Nat. Geosci. 13, 87–93.

Class, C., Goldstein, S.L., 1997. Plume-lithosphere interactions in the ocean basins: constraints from the source mineralogy. Earth Planet Sci. Lett. 150, 245–260.

Class, C., Goldstein, S.L., Altherr, R., Bachèlery, P., 1998. The process of plume–lithosphere interactions in the ocean basins—the case of Grande Comore. J. Petrol. 39, 881–903.

Class, C., Goldstein, S.L., Stute, M., Kurz, M.D., Schlosser, P., 2005. Grand Comore Island: a well-constrained "low $^{3}He/^{4}He$" mantle plume. Earth Planet Sci. Lett. 233, 391–409.

Claude-Ivanaj, C., Bourdon, B., Allègre, C.J., 1998. Ra–Th–Sr isotope systematics in Grande Comore Island: a case study of plume–lithosphere interaction. Earth Planet Sci. Lett. 164, 99–117.

Cotten, J., Le Dez, A., Bau, M., Caroff, M., Maury, R.C., Dulski, P., Fourcade, S., Bohn, M., Brousse, R., 1995. Origin of anomalous rare-earth element and yttrium enrichments in subaerially exposed basalts: evidence from French Polynesia. Chem. Geol. 119, 115–138.

Courtillot, V., Jaupart, C., Manighetti, I., Tapponnier, P., Besse, J., 1999. On causal links between flood basalts and continental breakup. Earth Planet Sci. Lett. 166, 177–195.

Debeuf, D., 2004. Etude de l'évolution volcano-structurale et magmatique de Mayotte (Archipel des Comores, Océan Indien): approches structurale, pétrographique, géochimique et géochronologique. Unpublished Ph. D. thesis Université de La Réunion 243.

Deino, A., Potts, R., 1992. Age-probability spectra for examination of single-crystal $^{40}Ar/^{39}Ar$ dating results: examples from Olorgesailie, southern Kenya Rift. Quat. Int. 13–14, 47–53.

Deniel, C., 1998. Geochemical and isotopic (Sr, Nd, Pb) evidence for plume–lithosphere interactions in the genesis of Grande Comore magmas (Indian Ocean). Chem. Geol. 144, 281–303.

de Saint-Ours, J., 1960. Etudes géologiques dans l'extre^me Nord de Madagascar et de l'Archipel des Comores. Thèse de Doctorat. In: Rapport Service géologique de Tananarive n°, vol. 221. Tananarive, Madagascar, p. 205.

Emerick, C.M., Duncan, R.A., 1982. Age progressive volcanism in the Comores Archipelago, western Indian Ocean and implications for Somali plate tectonics. Earth Planet Sci. Lett. 60, 415–428.

Emerick, C.M., Duncan, R.A., 1983. Errata to Age progressive volcanism in the Comores Archipelago, western Indian Ocean and implications for Somali plate tectonics. Earth Planet Sci. Lett. 62, 439.

Esson, J., Flower, M.F.J., Strong, D.F., Upton, B.G.J., Wadsworth, W.J., 1970. Geology of the comores archipelago, western Indian ocean. Geol. Mag. 107, 549–557.

Famin, V., Michon, L., Bourhane, A., 2020. The Comoros archipelago: a right-lateral transform boundary between the Somalia and Lwandle plates. Tectonophysics 789, 228539.

Feuillet, N., Jorry, S., Crawford, W.C., Deplus, C., Thinon, I., Jacques, E., Saurel, J.M., Lemoine, A., Paquet, F., Daniel, R., Gaillot, A., Satriano, C., Peltier, A., Aiken, C., Foix, O., Kowalski, P., Laurent, A., Beauducel, F., Grandin, R., Ballu, V., Bernard, P., Donval, J.P., Géli, L., Gomez, J., Pelleau, P., Guyader, V., Rinnert, E., Besancon, S., Bertil, D., Lemarchand, A., Van der Woerd, J., 2019. Birth of a large volcano offshore Mayotte through lithosphere-scale rifting. In: AGU Fall Meeting, V52D-01. San Francisco.

Feuillet, N., Jorry, S., Crawford, W.C., Deplus, C., Thinon, I., Jacques, E., Saurel, J.M., Lemoine, A., Paquet, F., Satriano, C., Aiken, C., Foix, O., Kowalski, P., Laurent, A., Rinnert, E., Cathalot, C., Donval, J.-P., Guyader, V., Gaillot, A., Scalabrin, C., Moreira, M., Peltier, A., Beauducel, F., Grandin, R., Ballu, V., Daniel, R., Pelleau, P., Gomez, J., Besancon, S., Géli, L., Bernard, P., Bachèlery, P., Fouquet, Y., Bertil, D., Lemarchand, A., Van der Woerd, J., 2021. Birth of a large volcanic edifice offshore Mayotte via lithosphere-scale dyke intrusion. Nat. Geosci. 1–9.

Flower, M.F.J., Strong, D.F., 1969. The significance of sandstone inclusions in lavas of the Comores archipelago. Earth Planet Sci. Lett. 7, 47–50.

Flower, M.F.J., 1971. Rare earth element distribution in lavas and ultramafic xenoliths from the Comores Archipelago, Western Indian Ocean. Contrib. Mineral. Petrol. 31, 335–346.

Flower, M.F.J., 1972. Petrology of volcanic rocks from Anjouan, comores archipelago. Bull. Volcanol. 36, 238–250.

Flower, M.F.J., 1973. Evolution of basaltic and differentiated lavas from Anjouan, comores archipelago. Contrib. Mineral. Petrol. 38, 237–260.

Fuhrmann, U., Lippolt, H.J., Hess, J.C., 1987. Examination of some proposed K-Ar standards: $^{40}Ar/^{39}Ar$ analyses and conventional K-Ar data. Chem. Geol. 66, 41–51.

Gee, M.J., Watts, A.B., Masson, D.G., Mitchell, N.C., 2001. Landslides and the evolution of El Hierro in the canary islands. Mar. Geol. 177, 271–293.

Germa, A., Quidelleur, X., Labanieh, S., Chauvel, C., Lahitte, P., 2011. The volcanic evolution of Martinique island: insights from K-Ar dating into the lesser antilles arc migration since the oligocene. J. Volcanol. Geoth. Res. 208, 122–135.

Gillot, P.-Y., Cornette, Y., 1986. The Cassignol technique for Potassium-Argon dating, precision and accuracy: exemples from the late Pleistocene to recent volcanics from southern Italy. Chem. Geol. Isot. Geosci. Sect. 59, 205–222.

Gillot, P.-Y., Cornette, Y., Max, N., Floris, B., 1992. Two reference materials, trachytes MDO- G and ISH-G, for argon dating (K-Ar and $^{40}Ar/^{39}Ar$) of Pleistocene and Holocene rocks. Geostand. Newsl. 16, 55–60.

Gillot, P.-Y., Hildenbrand, A., Lefevre, J.-C., Albore-Livadie, C., 2006. The K/Ar dating method : principle, analytical techniques, and application to Holocene volcanic eruptions in Southern Italy. Acta Vulcanol. 18, 55–66.

Guillou, H., Carracedo, J.C., Torrado, F.P., Badiola, E.R., 1996. K-Ar ages and magnetic stratigraphy of a hotspot-induced, fast grown oceanic island: El Hierro, Canary Islands. J. Volcanol. Geoth. Res. 73, 141–155.

Hajash, A., Armstrong, R.L., 1972. Paleomagnetic and radiometric evidence for the age of the Comores islands, west central Indian ocean. Earth Planet Sci. Lett. 16, 231–236.

Hildreth, W., Lanphere, M.A., 1994. Potassium-argon geochronology of a basalt-andesite-dacite arc system: the Mount Adams volcanic field, Cascade Range of southern Washington. Geol. Soc. Am. Bull. 106, 1413–1429.

Hogg, A.G., Heaton, T.J., Hua, Q., Palmer, J.G., Turney, C.S., Southon, J., et al., 2020. SHCal20 Southern Hemisphere calibration, 0–55,000 years cal BP. Radiocarbon 62, 759–778.

Lacroix, A., 1922. La constitution lithologique de l'archipel des Comores. C.R. XIIIeme congres Int. Géol. Bruxelles 2, 949–979.

Le Bas, M.J., Le Maitre, R.W., Streckeisen, A., Zanettin, B., IUGS Subcommission on the Systematics of Igneous Rocks, 1986. A chemical classification of volcanic rocks based on the total alkali-silica diagram. J. Petrol. 27, 745–750.

Lemoine, A., Briole, P., Bertil, D., Roullé, A., Foumelis, M., Thinon, I., Raucoules, D., de Michele, M., Valty, P., Hoste Colomer, R., 2020. The 2018–2019 seismo-volcanic crisis east of Mayotte, Comoros islands: seismicity and ground deformation markers of an exceptional submarine eruption. Geophys. J. Int. 223, 22–44.

Lenhardt, N., Oppenheimer, C., 2014. Volcanism in Africa: geological perspectives, hazards, and societal implications. *Extreme natural hazards, disaster Risks and societal implications*. Spl. Publ. Int. Union Geod. Geophysics 1, 169–199.

McDougall, I., 1971. The geochronology and evolution of the young volcanic island of Réunion. Indian Ocean. Geochim. Cosmochim. Acta 35, 261–288.

Masson, D.G., 1996. Catastrophic collapse of the volcanic island of Hierro 15 ka ago and the history of landslides in the Canary Islands. Geology 24, 231–234.

Montaggioni, L.F., Nougier, J., 1981. Les enclaves de roches detritiques dans les Volcans d'Anjouan (Archipel des Comores); Origine et interpretation dans le cadre de l'evolution du Canal de Mozambique. Bull. Soc. Géol. France 7, 595–601.

Michon, L., 2016. The volcanism of the Comoros Archipelago integrated at a regional scale p. 333-344. In: Active Volcanoes of the Southwest Indian Ocean. Springer-Verlag Berlin Heidelberg, p. 428.

Nougier, J., Cantagrel, J.M., Karche, J.P., 1986. The Comores archipelago in the western Indian Ocean : volcanology, geochronology and geodynamic setting. J. Afr. Earth Sci. 5, 135–145.

Pelleter, A., Caroff, M., Cordier, C., Bachèlery, P., Nehlig, P., Debeuf, D., Arnaud, N., 2014. Melilite-bearing lavas in Mayotte (France): an insight into the mantle source below the Comores. Lithos 208, 281–297.

Quidelleur, X., Gillot, P.Y., Carlut, J., Courtillot, V., 1999. Link between excursions and paleointensity inferred from abnormal field directions recorded at la Palma around 600 ka. Earth Planet Sci. Lett. 168, 233–242.

Quidelleur, X., Carlut, J., Soler, V., Valet, J.P., Gillot, P.Y., 2003. The age and duration of the Matuyama–Brunhes transition from new K–Ar data from La Palma (Canary Islands) and revisited $^{40}Ar/^{39}Ar$ ages. Earth Planet Sci. Lett. 208, 149–163.

Rabinowitz, P.D., Coffin, M.F., Falvey, D., 1983. The separation of Madagascar and Africa. Science 220, 67–69.
Raczek, I., Stoll, B., Hofmann, A.W., Peter Jochum, K., 2001. High-precision trace element data for the USGS reference materials BCR-1, BCR-2, BHVO-1, BHVO-2, AGV-1, AGV- 2, DTS-1, DTS-2, GSP-1 and GSP-2 by ID-TIMS and MIC-SSMS. Geostand. Newsl. 25, 77–86.
Rollinson, H., 1993. Using Geochemical Data: Evaluation, Presentation, Interpretation. Longman, Harlow, p. 352.
Samper, A., Quidelleur, X., Lahitte, P., Mollex, D., 2007. Timing of effusive volcanism and collapse events within an oceanic arc island: basse-Terre, Guadeloupe archipelago (Lesser Antilles). Earth Planet Sci. Lett. 258, 175–191.
Schwarz, W.H., Trieloff, M., 2007. Intercalibration of ^{40}Ar–^{39}Ar age standardsNL-25, HB3gr hornblende, GA1550, SB-3, HD-B1 biotite and BMus/2 muscovite. Chem. Geol. 242, 218–231.
Spath, A., Roex, A.P.L., Duncan, R.A., 1996. The geochemistry of lavas from the gomores archipelago, western Indian ocean: petrogenesis and mantle source region characteristics. J. Petrol. 37, 961–991.
Steiger, R.H., Jager, E., 1977. Subcommission on Geochronology: convention on the use of decay constants in Geo and Cosmochronology. Earth Planet Sci. Lett. 36, 359–362.
Strong, D.F., 1972. The petrology of the lavas of Grande Comore. J. Petrol. 13, 181–218.
Sun, S.S., McDonough, W.F., 1989. Chemical and isotopic systematics of oceanic basalts: implications for mantle composition and processes. Geol. Soc. Lond. Spec. Publ. 42, 313–345.
Thompson, R.N., Flower, M.F.J., 1971. One-atmosphere melting and crystallization relations of lavas from Anjouan, comores archipelago, western Indian ocean. Earth Planet Sci. Lett. 12, 97–107.
Tzevahirtzian, A., Zaragosi, S., Bachèlery, P., Biscara, L., Marchès, E., 2021. Submarine morphology of the Comoros volcanic archipelago. Mar. Geol. 432, 106383.
White, S.M., Crisp, J.A., Spera, F.J., 2006. Long-term volumetric eruption rates and magma budgets. Geochem. Geophys. Geosyst. 7.